Microwave Absorption in a Plasma Resonator operated with Hydrogen

G. Himmel and M. Osterhold
Institut für Experimentalphysik II, Ruhr-Universität Bochum, Bochum

Z. Naturforsch. **40 a**, 1220–1227 (1985); received September 27, 1985

The permeation of microwave pulses ($f = 9.4$ GHz, pulse duration: 0.5–0.7 μs) through a partially ionized hydrogen plasma is investigated. At supercritical electron densities (line-averaged density: $n_e = 1.2-1.8 \times 10^{18}$ m^{-3}) a resonant enhancement of the wave amplitude is observed between the plasma column and the metallic end reflector of the waveguide. Local measurements of the electric field strength in the cut-off layer next to the end reflector are correlated with the transient behaviour of the H_β line intensity, of the electron density, and of the mean electron energy. From these measurements, both the reduced H_β excitation rate and the reduced ionization rate by electron collisions are obtained as functions of the reduced effective field strength in the range 30–65 Vm^{-1} Pa^{-1}.

Introduction

In the past much effort has been made to model the rf-power dissipation in partially ionized plasmas [1–3], but practical applicability has only been demonstrated in a few cases. Moreover, the observed anomalous absorption of rf-waves in overdense plasmas has raised many new questions [4]. Most detailed information is expected from studying the time evolution of the electron energy distribution function. But this is hampered by many experimental and theoretical difficulties. Therefore it is preferable to confine oneself to cases which are easy to treat, neglecting diffusion losses and balancing the energy gain of electrons with the energy loss by inelastic collisions. This has been done in the work of Cottingham and Buchsbaum [2]. In addition, they presumed a negligible influence of the plasma properties on the propagation of microwaves. This condition has to be fulfilled if the electric field strengths are determined from the forward power fed into the empty microwave line. Although a simple procedure like this may be suitable for the breakdown phase of the microwave discharge, it generally cannot be employed in the case of a fully developed plasma reaching overcritical densities. The latter case is treated in the present work. In contrast to [2], the microwave amplitude inside the plasma was almost tripled by resonant enhancement. Therefore a quite different method for the determination of local rf-electric field strengths had to be applied.

Reprint requests to M. Osterhold, Institut für Experimentalphysik II der Ruhr-Universität Bochum, Postfach 10 21 48, D-4630 Bochum.

I. Theory

Considering plasma interaction with an rf-field under stationary conditions, a differential equation may be derived from the Boltzmann equation which is solved by the isotropic part $f(u)$ of the electron distribution function varying with the energy u. The solution becomes easier if the elastic electron collision frequency ν is independent of u (Brown, McDonald [5, 6]). In the case of atomic hydrogen and a weakly ionized plasma, this assumption is valid for energies above 5 eV ($\nu/p_H = 1.8 \times 10^7$ s^{-1} Pa^{-1}; $p_H = p$ in the following, i.e. p is twice the filling pressure measured at a temperature of 273 K). Generally, the electron energy distribution function is required for different values of the reduced effective field strength E_e/p. The latter is given by the relation

$$E_e = E_0 \nu/[2(\nu^2 + \omega^2)]^{1/2}, \quad (1)$$

where E_0 is the amplitude of the rf-field and ω is the angular frequency of the wave. Moreover, it is assumed that the efficiency h of inelastic processes (defined in [6]) is linearly dependent on the amount of electron energy which is in excess of the excitation threshold $h = 1.2 \times 10^{-2}(u/\text{eV} - 10.15)$. For

0340-4811 / 85 / 1200-1220 $ 01.30/0. – Please order a reprint rather than making your own copy.

high energies ($u > 25$ eV) this assumption leads to an overestimation of inelastic energy losses. On the other hand, the assumption of constant ν fails to be valid for $u < 5$ eV. Therefore the electron distribution function in the range $u < 5$ eV is set to the constant value $f(u = 5\text{ eV})$ before dividing all values of $f(u)$ by a suitable normalization factor. This treatment is justified as long as the distribution function is only used for the calculation of the average of a quantity which vanishes at low electron energies. The mean inelastic rates and the mean electron energy are given by the expressions

$$\bar{\nu}_{i,n} = N \int_{u_{i,n}}^{\infty} \sqrt{2u/m_e}\, Q_{i,n} f(u)\, du\,, \tag{2}$$

$$\bar{u} = \int_0^{\infty} u f(u)\, du\,, \tag{3}$$

where N is the ground state density of the neutrals; $Q_{i,n}$ denotes the cross section for ionization or excitation from the ground state; the threshold energy of each process is denoted by $u_{i,n}$ (n being the principal quantum number of the excited level). Analytical expressions for $Q_{i,n}$ may be found in [7]. Though the number density of electrons having energies above the excitation threshold is strongly influenced by variation of E_e/p, the mean electron energy $\bar{u}$ is not very sensitive to a change of this parameter. Actually, for E_e/p in the range $30-65\ \mathrm{V\,m^{-1}\,Pa^{-1}}$, the mean electron energy varies only in the range 5–7 eV. The problem of rf-power dissipation itself is tackled by setting up a power balance equation for the stationary state. For an average electron having the energy $\bar{u}$ the following relation is obtained:

$$\nu u_c = \bar{\nu}_i u_i + \sum_n \bar{\nu}_n u_n + (2m_e/M)\nu\bar{u} + \bar{u}/t_{diff} + \bar{u}/t_{heat}; \tag{4}$$

m_e is the electron mass, M the mass of a neutral; $u_c = (e^2 E_e^2/m_e)/\nu^2$ is the mean energy gain of a plasma electron between every two collisions. The right side of (4) describes the energy loss: (i) by ionization and excitation from the ground state, (ii) by elastic collisions with neutrals, and (iii) by convection and heat conduction. The latter processes are characterized by the loss rates t_{diff}^{-1} and t_{heat}^{-1}. After the rf-pulse has been switched on, it takes the time of the order of magnitude $\tau = \bar{u}/(u_c\nu)$ until a stationary state according (4) forms. But in the weakly ionized plasma a quasi-stationary state is also possible, which is determined by the balance between the energy gain in the rf-field and the losses by inelastic collisions. Approximately, the first two terms in (4) may be expressed by $u_x \bar{\nu}_{inel}$, where $\bar{\nu}_{inel} = \bar{\nu}_2 + \bar{\nu}_3 + \bar{\nu}_4 + \bar{\nu}_i$ and $u_x = 11.6$ eV. For later use, $\bar{\nu}_{inel}$ is written in the form $\bar{\nu}_i + c\,\bar{\nu}_4$; c is determined with the help of calculated distribution functions; it is only weakly dependent on E_e/p (see Table 1). Supposing a corona model is valid, the following relation between $\bar{\nu}_4$ and the intensity I of the line H_β is obtained:

$$\bar{\nu}_4 = [4\pi(I/L)/(n_e h\nu_{42} A_{42})] \sum_{k=1}^{3} A_{4k}\,, \tag{5}$$

where A_{4k} is Einstein's coefficient for spontaneous emission, $h\nu_{42}$ is the photon energy for the transition $n = 4 \rightarrow n = 2$, and n_e is the electron density. I/L is the total emission coefficient of the line, L being the depth of the emitting plasma layer. The value of $\bar{\nu}_i$ is given by the increment of the electron density at constant $\bar{u}$:

$$n_e = n_e^0 \exp(\bar{\nu}_i t); \tag{6}$$

here, n_e^0 is the electron density at the begin of the rf-pulse. As will be shown later on, this work refers to conditions under which the transition to the quasi-stationary state just mentioned is observed ca. 0.4 μs after the begin of the rf-pulse. The influence of a magnetic field orientated parallel with the rf-field is properly taken into account by an increase of the radial scaling lengths for diffusion and heat conduction, which corresponds to an increase of the energy confinement time scales t_{diff} and t_{heat}. For the purpose of a quantitative treatment, suitable expressions are available from transport theory.

Table 1. Parameter c occurring in the approximation $\bar{\nu}_{inel} = \bar{\nu}_i + c\,\bar{\nu}_4$ as a function of the reduced effective field strength E_e/p.

$\frac{E_e}{p}$ / ($\mathrm{Vm^{-1}\,Pa^{-1}}$)	37.6	45.1	60.2	75.2
c	29.7	27.6	26.7	26.0

II. Experiment

X-band microwave pulses ($\omega/2\pi = 9.4$ GHz; pulse duration: 0.5–0.7 μs) were launched into a hydro-

gen target plasma. The latter was generated by S-band microwave pulses in a spatially separated part of the discharge tube ($\omega/2\pi = 2.4$ GHz, pulse duration: 500 µs). Both microwave pulses were overlapping in time. A magnetic field ($B = 0.087$ T) was set up in a parallel direction either with the axis of the discharge tube and with the electric field of the X-band wave. By this magnetic field, the ECR condition for the S-band microwaves was fulfilled. A detailed description of the whole device was given in previous papers (Böhm [8], Böhm and Himmel [9]). With regard to the low filling pressure (0.4–1.0 Pa), a comparatively high electron density ($1.2-1.8\times10^{18}$ m^{-3}) exceeding the cut-off density of X-band waves was obtained. For this reason, the resonant enhancement of the TE_{10}-mode between the metallic end reflector of the X-band waveguide and the overdense plasma column could be maintained nearly during the whole X-band pulse. Postionization of the neutral background during the X-band pulse was reduced to a tolerable level so it did not lead to a fast detuning of the resonator as observed previously. The reproducibility of the S-band discharge was considerably improved by the hf-preionization; the latter was periodically switched off in the time of X-band activation in order to prevent hf-interference in the electronic devices during the measurements. For the high repetition rate of the S-band pulses (100 Hz) and for the operation of the hf-discharge between them, the filling gas was supposed to be completely dissociated. This assumption was confirmed by the emission spectrum in the range 270–500 nm. The level of molecular background radiation never reached the intensity of the Balmer line H_{11} which was the last detectable member of the Balmer series. Figure 1 shows the optical set-up used for the measurement of line intensities. The optical path was orientated at right angles to the X-band waveguide and to the electric field of the X-band wave. The radiation emitted from the cut-off layer of the plasma left the waveguide through an aperture of 4 mm diameter and then was led to the input slit of a spectrometer. By moving the output slit along the focal plane, a spectral range of 0.7 nm could be scanned. The outgoing radiation was detected by a photomultiplier (EMI 6256 S). Subsequently, the single photon pulses were given to a fourfold fan-out unit and counted in four different channels A–D. All counters were supplied with gate pulses of equal length. But

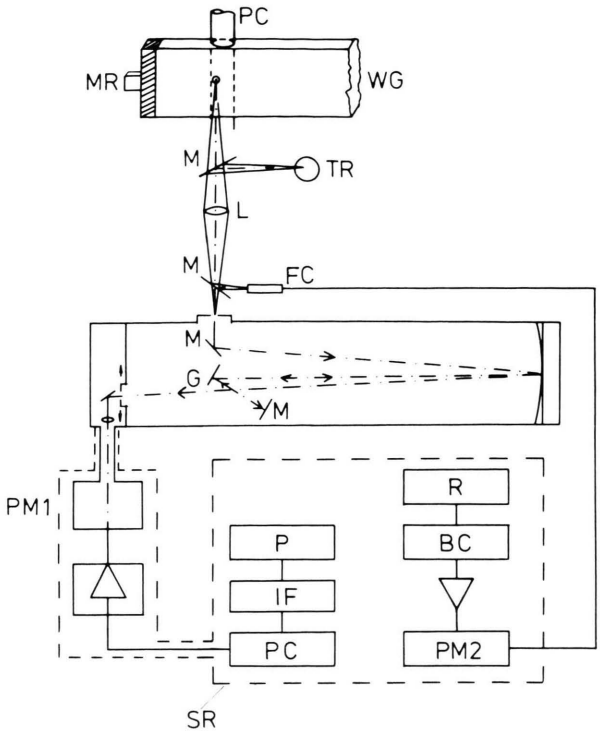

Fig. 1. Optical set-up: PC plasma column, WG X-band waveguide, MR metallic end reflector, M mirror, TR tungsten ribbon, L lense, FC fiber cable, G grating, PM photomultiplier, PC photon counter, IF interface unit, P printer, BC box-car integrator, R recorder, SR screened room.

the opening periods of the channels A and B were time delayed by 0.5–0.7 µs one in respect to the other and the same delay time was chosen between the channels B and C and between C and D. In channel A the photon events just before the X-band pulse were gathered, channel B was coincident with the microwave pulse, and the light emitted after the rf-pulse was measured in the channels C and D. After a preselected time, the contents of all counters were printed out. During the measurements, the exit slit of the spectrometer was tuned continuously over the profile of the spectral line H_β. Typically a spectral range of 2.5 pm was scanned within the period of one measuring cycle. By insertion of a mirror in front of the entrance slit, the light emitted from the same plasma volume was given to another photomultiplier (RCA 1P21). Its output was connected with a box-car integrator which measured the transient behaviour of the plasma light during and after the X-band pulse. The resonant enhancement of the X-band wave between the plasma

column and the metallic end reflector could be probed by a small antenna inside the cavity. The antenna signal was measured by a diode detector which was operated in the square-law regime. The total rf-power reflected by the plasma resonator was controlled with the help of a directional coupler connected with another square-law diode detector. Near the opening where the plasma column left the waveguide, an 8 mm-microwave interferometer was installed. A suitable choice of the initial interferometer phase provided nearly linear response and maximum sensitivity for measuring the line-averaged electron density. The variation $\Delta\bar{u}$ of the mean electron energy was controlled by means of a diamagnetic loop. The coefficient of self-inductance of this device amounted to 2.1 μH. For the evaluation of $\Delta\bar{u}$, the induced potential was processed in two different ways: (i) the voltage across an outer resistance of 46 Ω was time integrated; (ii) the current carried against the internal resistance of the short-circuited loop was used as a direct measure of $\Delta\bar{u}$. For periods as short as the X-band pulse width and for small variations of the electron density during the pulse, both methods delivered consistent results. Table 2 gives a summary of the most important experimental parameters in comparison with the work of Cottingham and Buchsbaum [2]. It should be noted that in the latter work the electric rf-field was orientated perpendicular to the axis of the discharge tube whereas it was parallel in our case.

Table 2. Comparison of the experimental parameters of this work with [2].

	Cottingh., Buchsb.	our experiment
$n_e / 10^{18}\,m^{-3}$	< 0.05	1.2 - 1.8
filling pressure p_{H_2} / Pa	130 - 1300	0.4 - 1.0
$E_0 / 10^5$ V/m	0.2 - 1.2	1.4 - 3.1
f / GHz	3.02	9.4
pulse duration / μs	1 - 2	0.5 - 0.7
discharge tube diameter / mm	10	22
waveguide dimensions / mm	72 × 34	29 × 70

III. Experimental Results

The Figs. 2 and 3 present the time characteristics of various signals picked up during and after the X-band pulse and smoothed by means of a box-car integrator. The resonant state manifested itself by the response of the antenna inside the cavity while the reflected power produced a signal pattern which was almost complementary to that coming from the plasma resonator. Within experimental accuracy, the onset of increased light emission from different sections of the discharge tube, inside and outside the resonator cavity, was simultaneous; it happened before the electron density increased considerably. Looking for an explanation, any coupled effect of plasma interaction with S-band and X-band microwaves could be excluded. For a check, the X-band

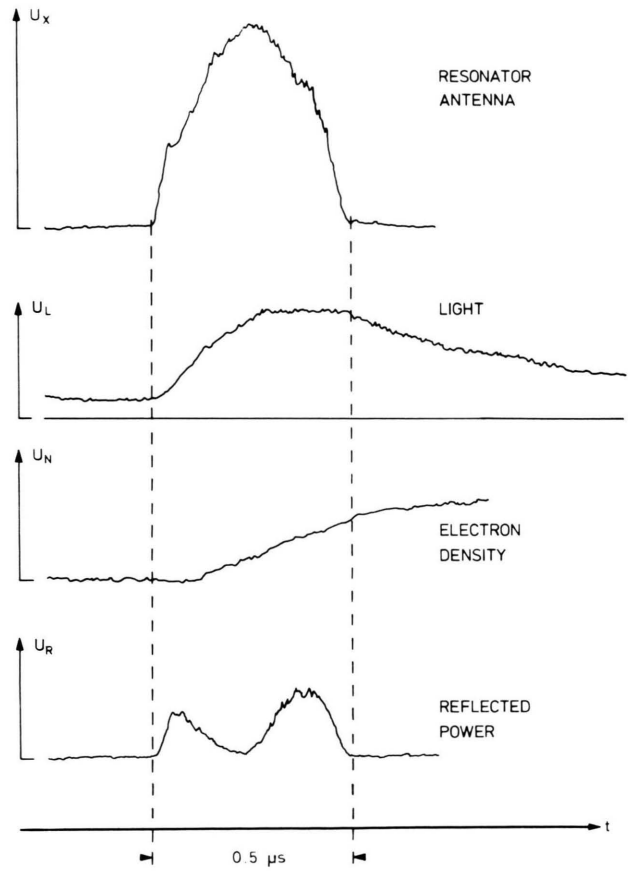

Fig. 2. Time characteristics of the plasma light and of the line-averaged electron density during the X-band pulse ($\sqrt{\overline{E_0^2}} = 2.1 \times 10^5$ V/m, $p_{H_2} = 0.5$ Pa, $n_e^0 = 1.4 \times 10^{18}$ m^{-3}).

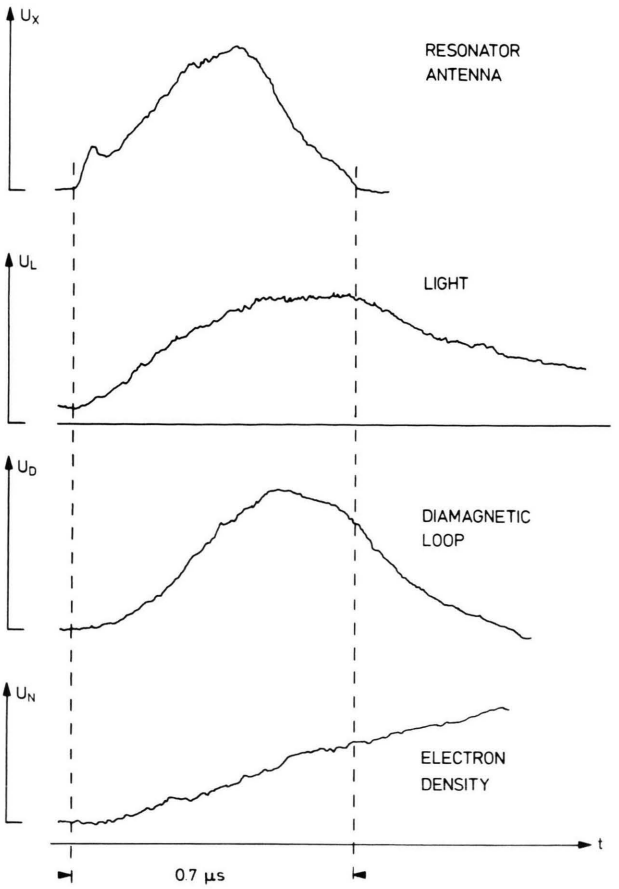

Fig. 3. Comparison of the time characteristics of the plasma light during the X-band pulse with the transients of the mean electron energy and of the line-averaged electron density ($\sqrt{\overline{E_0^2}} = 2.2 \times 10^5$ V/m, $p_{H_2} = 0.6$ Pa, $n_e^0 = 1.6 \times 10^{18}$ m^{-3}).

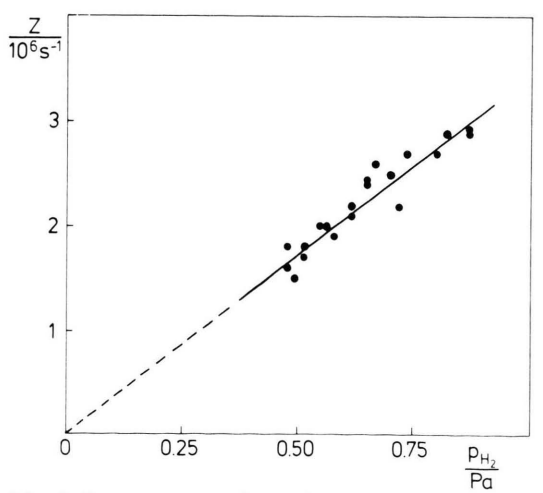

Fig. 4. Decay rate Z of the plasma light as a function of the filling pressure p_{H_2}.

pulse was triggered in the early afterglow phase, i.e. 3–10 µs after the end of the S-band pulse, without any alteration of the features given in Figure 2. From these findings it was concluded that heat conducting or/and another mechanism of fast energy transport parallel to the magnetic field prevented steep axial gradients of the mean electron energy transport parallel with the magnetic field prevented steep axial gradients of the mean electron tion to the quasi-stationary state mentioned in Sect. I appeared whereas the lapse of the X-band pulse was followed by a relatively slow decrease of light intensity. As shown in Fig. 4, the decay rates depended linearly on the filling pressure which supported the assumption of negligible diffusion and heat conduction in this state. The time characteristics of the diamagnetic current reflected the transient behaviour of the mean electron energy. In the records (see Fig. 3), the onset of inelastic losses was clearly marked. As an upper limit a mean electron energy of 10 eV was obtained from the peak value of the diamagnetic signal. This result was used for an estimate of the quantities t_{diff} and t_{heat} occurring in the power balance equation (4). In a direction parallel with the magnetic field (which also means parallel with the discharge tube) we obtained $t_{diff} \approx 2.5$ µs and $t_{heat} \approx 3.5$ µs. These estimates were based on a characteristic diffusion length of 7 cm which equaled the length of the discharge exposed to X-band waves, and on a characteristic heat conduction length of 50 cm corresponding to half the total length of the discharge tube. In a direction perpendicular to the magnetic field, we obtained $t_{diff} \approx 550$ µs and $t_{heat} \approx 350$ µs. In comparison with the observed decay time of the mean electron energy, these times were considerably larger, which again argued in support of neglecting heat conduction and diffusion in (4). During the X-band pulse the electron density did not increase more than 15–20% of its initial value. By this increase, however, the cut-off situation became more critical. Accordingly, the degree of coupling between the resonator cavity and the transmission line deteriorated substantially. In consequence of this, the rf-power density inside the cavity was strongly reduced towards the end of the X-band pulse, whereas the amount of reflected power increased. As to the observed transition to a quasi-stationary state, further information about electron energies was expected from a Boltzmann plot presenting the

density of bound electrons in an excited atomic state as a function of the binding energy (see Figure 5). Supposing a partial LTE by the way of a trial, an electron "temperature" of 0.2 eV was evaluated from the slope of the straight lines in the diagram. The large discrepancy between this value and the mean electron energy measured perpendicular to the magnetic field by means of the diamagnetic loop revealed a pronounced non-maxwellian character of the electron energy distribution. It was strongly suggested that the latter consisted of a low energy bulk determining the slope of the Boltzmann plot and a tail being the cause of large diamagnetic currents. This view was confirmed by the slow decay of the plasma light after the microwave pulse, which was traced back to the gradual deceleration of fast electrons. Figure 6 shows the broadening of the H_β line. The measurements were performed in channel B which was attributed to the time during which the rf-pulse was switched on, whereas the unperturbed line profiles in Fig. 6 were measured in the channels A, C, and D which were activated before and after the pulse. Actually, Blochinzew's theory [10] of the ac Stark effect predicted symmetrical line splittings. These splittings, however, could not be resolved because each component of a splitting pattern was influenced by Doppler and apparatus broadening, by fine structure and Zeeman splitting, and also by a slight Stark broadening which was produced by the plasma microfield. All these effects were properly taken into account by adjusting the width of each component to the width of the unperturbed line profile as it was obtained e.g. from measurements in channel D. For various rf-field strengths a whole set of line profiles was calculated from which the following relation between the line width $\Delta\lambda$ (FWHM in units of pm) and the electric field amplitude E_0 (in units of 10^5 V/m) was derived:

$$\Delta\lambda = 7.70\, E_0 + 3.88\, E_0^2 + \delta\lambda\,. \tag{7}$$

Here, $\delta\lambda$ is the width (FWHM) in pm of the unperturbed line. For a comparison with measured line widths, each of the quantities E_0, E_0^2, and $\Delta\lambda$ in (7) had to be replaced by its weighted time average.

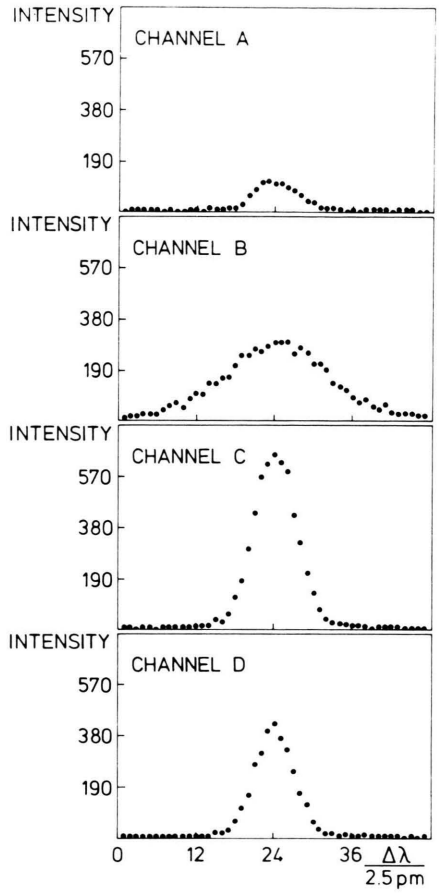

Fig. 6. Transient behaviour of the H_β line profile (λ 486 nm) at $\sqrt{\overline{E_0^2}} = 2.0 \times 10^5$ V/m ($p_{H_2} = 0.7$ Pa, $n_e^0 = 1.3 \times 10^{18}$ m^{-3}).

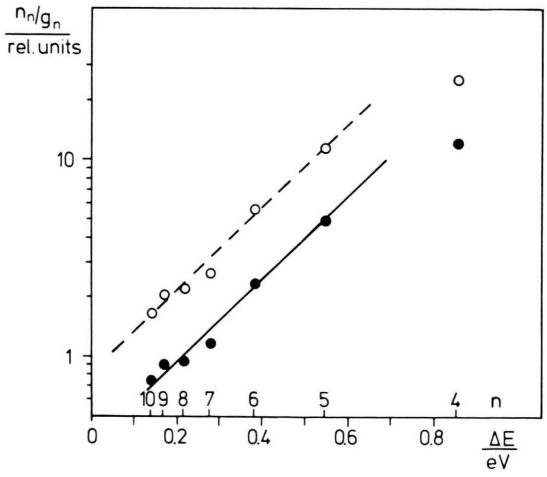

Fig. 5. Boltzmann plot: population density n_n in the excited state n (statistical weight g_n) with the X-band pulse switched on (open circles) and switched off (full circles) versus $\Delta E = u_i - u_n$; the slope of the linear portion of the curves yields the respective electron "temperature" ($\sqrt{\overline{E_0^2}} = 1.8 \times 10^5$ V/m, $p_{H_2} = 0.5$ Pa).

The weighting function was taken from the time characteristics of the plasma light during the X-band pulse. The relation between the weighted time average $\langle E_0 \rangle$ and $\langle E_0^2 \rangle$ was deduced from the time resolved detector signals associated with the rf-power densities inside the resonator cavity. Multiplication of the weighted time average $\langle E_0^2 \rangle$ with a conversion factor near 1 yielded the not weighted time average $\bar{E}_0^2$ which was required for the calculation of $\bar{E}_e^2$ with the help of (1). In the following the notation E_e explicitly refers to the quantity $(\bar{E}_e^2)^{1/2}$. Typically, the rf-electric field amplitudes determined from the ac Stark effect were in the range $1.4-3.1 \times 10^5$ V/m. In this range the accuracy of evaluation was limited to ca. $\pm$ 5%.

IV. Conclusion and Summary

The excitation rate $\bar{\nu}_4$ – in Fig. 7 it is divided by the pressure p of the atomic gas at a temperature of 273 K and plotted versus the reduced effective field strength E_e/p – was determined from (5) by measuring the total intensity of the line H_β in the quasi-stationary state and comparing its value – minus the initial value before the microwave pulse – with the amount of radiation emitted from a tungsten ribbon. The latter was used as a secondary radiation standard. For E_e/p in the range $30-55\ \mathrm{Vm^{-1}\,Pa^{-1}}$, the experimental rates were slightly higher than the rates calculated from (2). These deviations which were more pronounced at higher electric field strengths indicated that the calculated contribution of fast electrons was underestimated to some extent. A similar conclusion was drawn from the reduced ionization rate $\bar{\nu}_i/p$ plotted against E_e/p in Figure 8. In contrast to the former case, however, the discrepancies between experimental and theoretical values tended to become smaller at higher values of E_e/p. The experimental determination of $\bar{\nu}_i$ was based on the relation $\bar{\nu}_i = \mathrm{d} \ln n_e/\mathrm{d}t$ (cf. (6)) where the temporal derivative of $\ln n_e$ referred to a time near to the end of the X-band pulse. For the total rate of inelastic collisions the approximation $\bar{\nu}_{inel} = \bar{\nu}_i + c\,\bar{\nu}_4$ (with c from Table 1) was used. The reduced rate $\bar{\nu}_{inel}/p$ – depicted in Fig. 9 as a function of E_e/p – was compared with the expression $\bar{\nu}_{inel}/p = u_c \nu/(u_x p)$ which followed from the power balance (4), neglecting diffusion and heat conduction. In the considered range of E_e/p satisfactory agreement was found which implied that the choice of binary collision frequencies ν in (1) was reasonable; i.e. that there was no need to incorporate scattering from turbulent charge density fluctuations into (1). In other cases (e.g. see [11]), this collective effect was associated with an effective collision frequency being much enlarged in comparison with ν. From the angle of plasma diagnostics, the proportionality $\bar{\nu}_{inel} \sim u_c \sim E_0^2$ is worth emphasizing. Provided the ratio $\bar{\nu}_4/\bar{\nu}_{inel}$ is only weakly dependent on E_e/p, a correlation between the total line in-

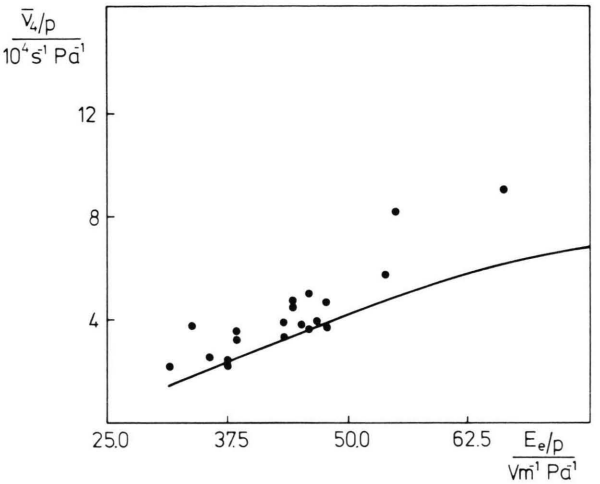

Fig. 7. Reduced excitation rate $\bar{\nu}_4/p$ according to (5) as a function of E_e/p in comparison with the theoretical curve according to (2) (solid line).

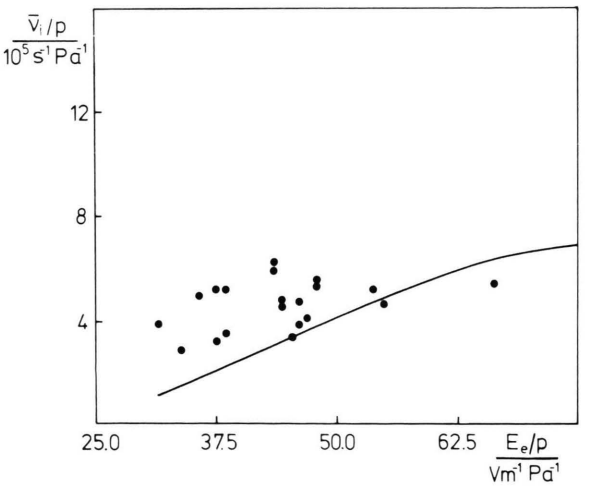

Fig. 8. Reduced ionization rate $\bar{\nu}_i/p$ according to (6) as a function of E_e/p in comparison with the theoretical curve according to (2) (solid line).

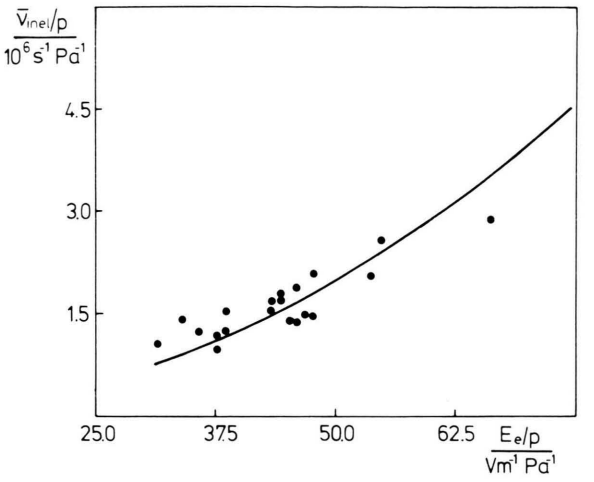

Fig. 9. Reduced total inelastic rate $\bar{\nu}_{inel}/p$ versus E_e/p compared with the expression $\bar{\nu}_{inel}/p = u_c\, \nu/(u_x\, p)$ resulting from the power balance equation (solid line).

tensity of H_β and the dissipated rf-power is established by additional use of (5). Under circumstances being incompatible with the use of material probes, a suitable evaluation of measured H_β line intensities may be considered as an alternative way to get some knowledge of the spatial distribution of the rf-power applied to the plasma. An example of such a case is given in [11]. In absence of diffusion and heat conduction, the power balance is governed by a more or less pronounced tail of fast electrons in the energy distribution, depending on the value of E_e/p. The relaxation of the perturbed energy distribution – after the electric field has been switched off – was calculated in detail by Wilhelm and Winkler [12]. According to [12], a fast decay of the non-maxwellian tail and its concentration at energies somewhat higher than the ionization limit is followed by a comparatively slow decrease of energies to values near the excitation threshold. The time scale of relaxation is in accordance with the time duration of 1–2 μs which was measured from the end of the X-band pulse up to the time when the plasma light had decayed to 10% of its maximum value. But a more detailed discussion of our experimental results with the help of [12] is questionable because the model refers to dc-electric fields and to a neutral background consisting of molecular hydrogen.

Acknowledgements

We are grateful to Professor Dr. H. Schlüter for valuable discussions and encouragement in this work. We are indebted to W. Hospodarz for technical assistance. The investigation was part of the joint efforts within the Sonderforschungsbereich 162 "Plasmaphysik Bochum/Jülich".

[1] W. P. Allis and S. C. Brown, Phys. Rev. **87,** 419 (1952).
[2] W. B. Cottingham and S. J. Buchsbaum, Phys. Rev. **130,** 1002 (1963).
[3] J. Marec, E. Bloyet, M. Chaker, P. Leprince, and P. Nghiem, in Electrical Breakdown and Discharges in Gases, E. E. Kunhardt and L. H. Luessen, eds., part B, Plenum Press, New York 1983.
[4] V. E. Golant and M. V. Krivosheev, Soviet Physics, Techn. Phys. **14,** No. 5, 719 (1969).
[5] S. C. Brown, Introduction to Electrical Discharges in Gases, John Wiley, New York 1966.
[6] A. D. MacDonald, Microwave Breakdown in Gases, John Wiley, New York 1966.
[7] H. W. Drawin, Rep. EUP-CEA-FC-383 Assoc. EURATOM-CEA (1967), Fontenay-aux-Roses, France.
[8] G. Böhm, Z. Naturforsch. **35 a,** 239 (1980).
[9] G. Böhm and G. Himmel, Appl. Phys. **21,** 313 (1980).
[10] D. I. Blochinzew, Phys. Z. Sowjetunion **4,** 501 (1933).
[11] G. Himmel and A. Kamp, Plasma Physics **27,** No. 4, 457 (1985).
[12] J. Wilhelm and R. Winkler, J. Physique, Colloque **C7,** 251 (1979).